Topography Mapping With a Portable Real-Aperture Radar Interferometer

Tazio Strozzi, *Senior Member, IEEE*, Charles Werner, *Senior Member, IEEE*, Andreas Wiesmann, *Senior Member, IEEE*, and Urs Wegmüller, *Senior Member, IEEE*

***Abstract*—In this letter, the requirements to derive topography from a portable terrestrial radar interferometer are introduced, the instrument design and the relationship between interferometric phase shift and surface topography are explained, and two examples of topographic maps from measurements at the Rhone glacier and Grabengufer rock glacier in Switzerland are presented. In the first case, an external digital elevation model was used to assess the error of topography mapping with the portable radar interferometer and to analyze ice surface changes of the glacier in the last 14 years. We found that the height error standard deviation is about 3 m within a distance of 2 km from the sensor and observed massive thinning of the Rhone glacier. In the second case, we used the terrestrial radar interferometer in order to measure the height difference between August 2009 and March 2010 over the rock glacier as a consequence of its destabilization.**

***Index Terms*—Digital elevation model (DEM), glacier, radar, radar interferometry.**

I. Introduction

RADAR interferometric techniques have been widely used with satellite data to produce global digital elevation models (DEMs). Most of the DEMs reconstructed from satellite radars used data from the European Remote Sensing (ERS) satellites ERS-1 and ERS-2 during the tandem phase between 1995 and 2000 with one-day acquisition time interval and from the single-pass Shuttle Radar Topography Mission (SRTM) during an 11-day campaign in February 2000. In the case of the ERS-1/2-derived DEMs, the vertical error is typically a few tens of meters [1], [2], although relative errors of a few meters were also reported [3], [4]. The planimetric resolution of the ERS-derived DEMs is about 25 m. The indicated absolute and relative 90% vertical accuracies of the SRTM DEM are ± 16 and ± 6 m, respectively, whereas the horizontal positional accuracy is about ± 20 m [5], [6]. Both ERS and SRTM DEMs show sections without data because of radar shadow, layover, and insufficient interferometric coherence.

Although, at a local scale, terrestrial radar interferometers are also employed to derive the surface topography of the illumination area. A quick topographic reconstruction, even with incomplete spatial coverage, may be, for instance, employed for the identification of landslide or glacier hazard. In addition, the availability of topographic information permits precise *in situ* localization of terrestrial radar images. In comparison to satellite radar interferometry, in the case of ground-based data, long repeat times can be avoided, and the number of views of the scene can be arranged. First studies on topography mapping with a ground-based synthetic-aperture radar at C-band [7]–[10] indicate an absolute error of about 5 m within a distance of 2 km from the sensor.

Fig. 1. GPRI overlooking the Rhone glacier in the Valais region of Switzerland on September 6, 2007.

In 2007, Gamma Remote Sensing developed and constructed a portable imaging terrestrial radar interferometer operating at 17.2 GHz [11], [12]. Unlike other ground-based systems based on azimuth resolution by synthetic aperture, the radar utilizes an azimuthal rotating interferometric array of real-aperture antennas. This allows having a mobile instrument that is able to illuminate an angular sweep of up to 360° in a short time. The main purpose of the radar interferometer is the monitoring of unstable slopes. However, the receiving system, as shown in Fig. 1, includes dual antennas to form a spatial interferometric aperture. Because two images are created simultaneously, an elevation model of the entire scene, including rapidly decorrelated targets as forest, can be created; there are no atmospheric artifacts; and there is no need to separate motion from topography. Multiple acquisitions to reduce errors are easily possible, owing to the rapid acquisition time.

In a first part of this letter, the terrestrial radar is presented. The theoretical bases of topographic reconstruction with radar interferometry are then given. This section also includes considerations about possible sources of errors. In the following, an example of topography reconstruction from radar

Manuscript received February 3, 2011; revised April 1, 2011, June 1, 2011, and July 27, 2011; accepted August 17, 2011. Date of publication October 6, 2011; date of current version February 8, 2012. This work was supported in part by the European Commission Sixth Framework Program Project GALAHAD (018409) and in part by the Swiss Federal Office for the Environment.

The authors are with Gamma Remote Sensing, 3073 Gümligen, Switzerland (e-mail: strozzi@gamma-rs.ch; cw@gamma-rs.ch; wiesmann@gamma-rs.ch; wegmuller@gamma-rs.ch).

Digital Object Identifier 10.1109/LGRS.2011.2166751

measurements of the Rhone glacier (Switzerland) with an assessment of the error by comparison with an available external DEM is presented. The external DEM is also used to analyze the ice surface height changes of the glaciers in the last 14 years. Finally, measurements with the terrestrial radar interferometer of the rapid topographic change over a destabilized rock glacier in the Swiss Alps are discussed.

II. GPRI

The Gamma portable radar interferometer (GPRI) (see Fig. 1) is a frequency-modulated continuous-wave radar operating in the frequency range of 17.1–17.3 GHz with an output power of +18 dBm [11], [12]. The slant-range resolution of the system is

$$\delta r = \frac{c}{2B}. \tag{1}$$

The chirp bandwidth of 200 MHz yields a nominal range resolution of 0.75 m. The azimuth antenna pattern determines the GPRI azimuth resolution. The nominal 3-dB beamwidth of the antenna is 0.4°, which is equivalent to a resolution of 7.5 m at a 1-km distance. The antenna gain is 25 dB with an elevation beamwidth of 45°.

The radar microwave electronics are mounted physically close to the antennas on the support structure in order to reduce feed losses. The antenna spacing is 25 cm between the receive antennas, with the transmit antenna located 35 cm above the center receiving antenna. A rigid carbon fiber truss is used to maintain antenna alignment. The separate transmit antenna is required to obtain sufficient isolation between receive and transmit channels. The antenna tower is attached to a mount that is responsible for azimuth positioning. A typical data acquisition covers an angular sweep of about 90°; however, full 360° imaging is possible. This is a major advantage of polar scanning over linear rail-based systems. The azimuthal pointing angle is repeatable with an accuracy of better than 0.04°. The scan time for a 90° sweep was approximately 30 min and was limited by the mount. The entire radar is controlled by a laptop computer via a Universal Serial Bus interface.

Processing of the individual images requires windowing of the echoes followed by a fast Fourier transform. It is also important for generation of DEM data that the video filters in the upper and lower channels are close to identical with respect to phase and group delays in order to suppress relative phase errors between the channels. The data are collected and processed in polar format and can be resampled into rectangular or terrain geocoded format using bicubic spline interpolation.

III. Relationship Between Interferometric Phase Shift and Surface Topography

As shown in Fig. 2, a radar signal of the interferometer is transmitted from antenna A_1 and received at both antennas A_2 and A_3 separated by a vertical baseline B to form an interferogram. Using the laws of sine and cosine, we can determine the following equations for the surface topography z as a function

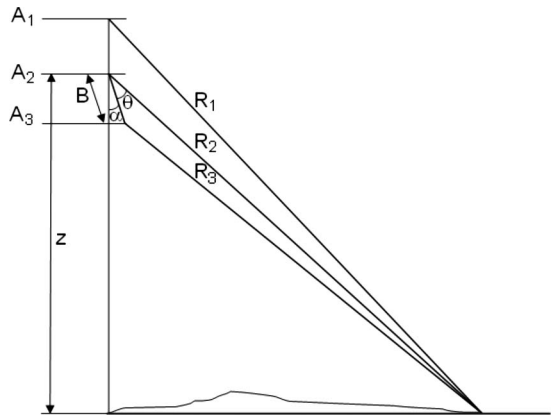

Fig. 2. Interferometer imaging geometry. A radar signal is transmitted from antenna A_1 and received at both antennas A_2 and A_3 separated by a baseline B to form an interferogram.

of the ranges to a point on the ground R_2 and R_3 and the look and baseline angles θ and α [3]:

$$\cos(\theta + \alpha) = \frac{z}{R_2} \tag{2}$$

$$R_3^2 = B^2 + R_2^2 - 2BR_2\cos\theta. \tag{3}$$

The difference in path lengths from the transmitting antenna A_1 to a point on the ground and back to the receiving antennas A_2 and A_3 is related to the measured interferometric phase ϕ and wavelength λ of the radar by

$$\phi = -\frac{2\pi}{\lambda}(R_3 - R_2). \tag{4}$$

If the interferometer is set up perfectly vertical $(\alpha = 0)$, the following expression results for the surface topography z as a function of the interferometric phase ϕ from (2)–(4):

$$z = \frac{\lambda}{2\pi}\frac{R_2}{B}\phi + \frac{B}{2} - \left(\frac{\lambda}{2\pi}\right)^2 \frac{\phi^2}{2B}. \tag{5}$$

The height of ambiguity [13], i.e., the height resulting in a phase change of one fringe (2π), is about 150 m at 2-km range for a baseline of 0.25 m. For most typical surface terrains in hilly areas, a baseline of 0.25 m seems a reasonable value to avoid phase unwrapping problems and still have a relatively high sensitivity to height changes.

The principal errors associated with the measurements arise from uncertainties in the measured phase ϕ, the baseline B, and the angle α of the baseline with respect to the vertical. The propagation through the atmosphere can be neglected because the two images of the interferogram are acquired simultaneously.

Differentiation of (5) with respect to the interferometric phase ϕ and without considerations of the nonlinear term yields the error in height estimate as a function of the error in phase estimate

$$\sigma_z = \frac{\lambda}{2\pi}\frac{R_2}{B}\sigma_\phi. \tag{6}$$

For a phase standard deviation of 10°, corresponding to a coherence of about 0.95 for one radar look, the height standard deviation is about 4 m at 2-km distance.

Differentiation of (5) with respect to the baseline B yields the error in height estimate as a function of the error in the baseline

$$\sigma_z = \left(\left(\frac{\lambda}{2\pi} \right)^2 \frac{\phi^2}{2B^2} - \frac{\lambda}{2\pi} \frac{R_2}{B^2} \phi + \frac{1}{2} \right) \sigma_B. \tag{7}$$

An error in the determination of the baseline of 0.1 cm yields a height error of about 1 m at a distance of 3 km in the case of a phase change of one fringe (2π).

Differentiation of (2) with respect to the baseline angle α yields the error in height estimate as a function of the error in the baseline angle

$$\sigma_z = R_2 \sin(\theta + \alpha) \sigma_\alpha. \tag{8}$$

An error in the estimation of the baseline angle of 0.1° yields in the case of a constant look angle $(\theta + \alpha)$ of 45° a height error of about 1 m at a distance of 3 km.

Typical expected topographic errors are thus a few meters for distances up to 2 km, and extremely precise knowledge of the baseline geometry is required for an absolute height estimation. It is important to notice that the two types of errors—phase standard deviation and baseline geometry—are different in nature [3]. The phase errors increase the statistical variation of each point of the DEM, while the baseline geometry errors are systematic in the sense that a sort of tilt across the radar swath is introduced. The latter can be corrected using knowledge of the height of a few ground control points.

IV. Experiment at the Rhone Glacier

An experiment at the Rhone glacier in the Swiss central Alps was conducted on September 6, 2007. This glacier has been selected because it can be directly reached from the Furka pass street and has been already the subject of various studies [14]. Fig. 1 shows the setup of the instrument over the glacier. The experiment was principally performed to derive the surface velocity of the glacier. However, with its dual receiving antennas, the terrestrial radar interferometer also permits creating an elevation model. A total of ten single-pass interferometric pairs were measured within about 4 h with an acquisition interval of one scan on the order of 20 min. The array of antennas was rotated on the azimuthal axis by 50° in spacing of 0.1° in order to illuminate both ice-free sides of the glacier. Processing of the raw radar data to single-look complex images was done up to a slant-range distance of 2250 m. An incoherent average of the 20 images (ten from each of the upper and lower antennas) was done for speckle reduction and is shown in Fig. 3. The image is displayed in the original radar slant-range–azimuth-angle coordinates with the average of two looks in slant range. The border of the glacier and the crevasses are well visible in the figure.

Single-pass interferograms were computed with two looks in slant range and one look in azimuth (see one example in Fig. 3). Only very small differences could be observed between the ten interferometric pairs. The fringes are very well preserved over the rocky areas and the steeper part of the glacier up to a distance of about 1 km, where the coherence is generally higher than 0.95. For the remote part of the glacier, characterized by a flatter topography, the coherence is on the order of 0.7–0.8. As expected, phase decorrelation is observed over areas of shadow. In order to help unwrap the phase of the interferograms, a nonlinear filtering was applied [15]. Phase unwrapping was then performed with a region growing algorithm [16] for points characterized by coherence values larger than 0.9. In the following step, the filtered unwrapped phase was used as a model in order to unwrap the unfiltered interferograms. An average of all ten unfiltered and filtered interferograms was applied. Finally, the unwrapped phase was converted to surface topography using (2)–(4). A baseline B of 0.25 m and a baseline angle α of 4.1° were determined by using ground control points on rocky areas extracted from an external DEM and minimizing the difference between real and reconstructed heights. The ground control points were also employed to determine the constant height offset.

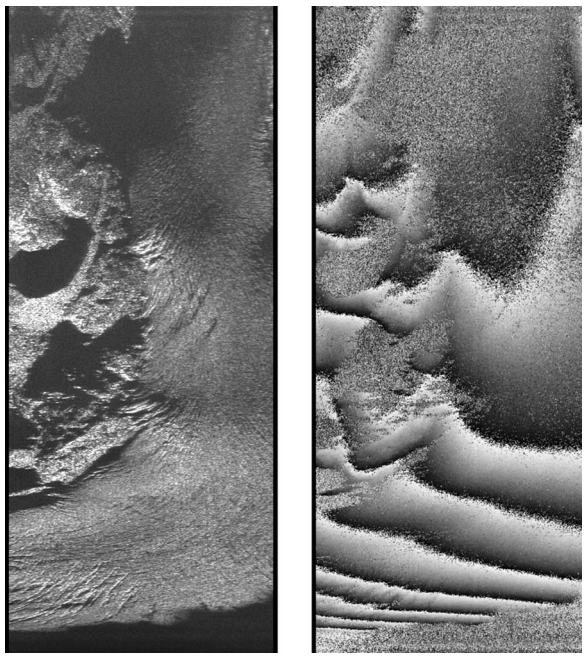

Fig. 3. (Left) Intensity image and (right) single-pass interferogram of the Rhone glacier on September 6, 2007, in the original radar geometry.

Fig. 4 shows the height difference between the GPRI DEM computed from the average of ten filtered interferograms and an external DEM derived from aerophotogrammetry (DHM25). For the Rhone glacier, the contour lines for deriving the external DEM with a spatial resolution of 25 m were updated in 1993, with an estimated vertical accuracy of 3 m. The surface topography determined by the GPRI only covers a small section of the Rhone glacier, but massive glacier thinning during the past 14 years can be observed. Extreme thickness losses of more than 40 m were measured toward lower elevations. This is in general accordance to direct mass balance measurements [14] and glacier elevation changes from DHM25 and the SRTM DEM [17].

For the ice-free region to the west of the Rhone glacier, histograms of the height differences between the GPRI and the external DEMs were computed at distances from about 700 to 1200 m and from about 1300 to 2000 m and are shown in Fig. 5. By considering the average of ten filtered interferograms, the

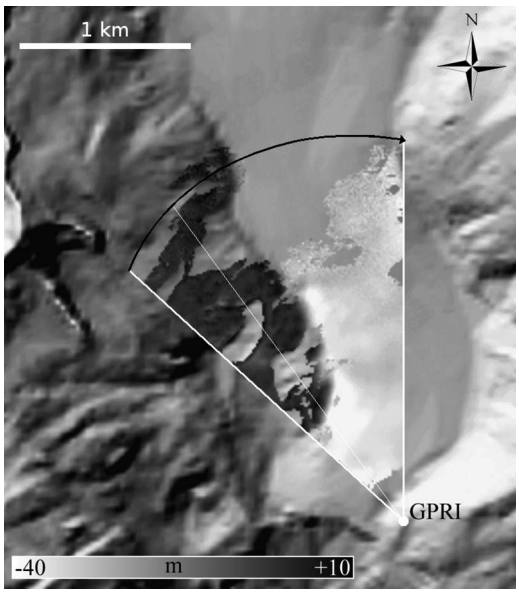

Fig. 4. Height difference between the surface topography of the Rhone glacier determined from the terrestrial radar interferometer by the average of ten filtered interferograms and an external DEM. The shaded relief of the external DEM is used as image background. The thin line represents azimuth scan 130, where the profile of Fig. 6 has been extracted.

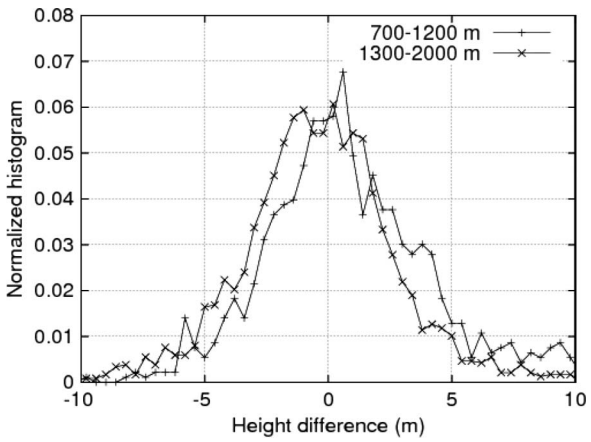

Fig. 5. Normalized histograms of the height difference between the GPRI and external DEMs for the ice-free region to the west of the Rhone glacier. The GPRI DEM was determined by the average of ten filtered interferograms. The minimum and maximum distances to the sensor were 700 and 1200 m and 1300 and 2000 m, respectively.

height differences are within ± 10 m, with standard deviations of 3.4 m at the shorter range and 3.3 m at the larger range. After the filter and average of multiple interferograms, the error of the GPRI DEM is not dominated by the phase noise. The reasons for the difference between the GPRI and the external DEMs for the ice-free region are as follows: 1) residual uncertainties in the estimation of the baseline and the baseline angle, e.g., visible in the shifted mean of the histograms with respect to zero; 2) different resolutions of the two DEMs, also considering the spatial filtering applied to the terrestrial radar data; 3) the quality of the external DEM, which has an estimated vertical accuracy of 3 m; and 4) the different viewing geometries of the two DEMs, with the airborne DEM less appropriate to reconstruct the topography of relatively steep slopes which are better illuminated by the GPRI. For a single filtered interferogram,

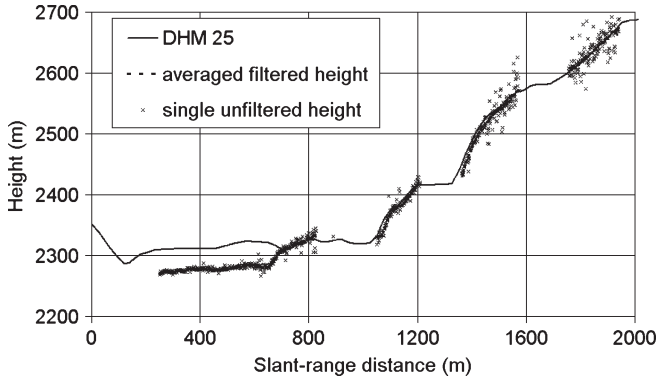

Fig. 6. Profiles of the GPRI and DHM25 heights along azimuth line 130 (for position, see Fig. 4).

on the other hand, the height standard deviations are 4.6 m at distances from about 700 to 1200 m and 7.5 m at distances from about 1300 to 2000 m, with an increased error at larger distances as suggested by (6).

The height profiles for azimuth line 130 (the scan is from left to right; see Fig. 4) were compared with the profile extracted along the same direction from the external DEM. Fig. 6 shows the results for a single unfiltered interferogram and for the average of all ten filtered interferograms. The profile of the DHM25 heights was transformed from the horizontal distance to the distance along the radar line of sight. The retreat of the glacier from 1993 to 2007 between slant-range distances 250 and 700 m and the topography of the mountain behind the glacier are very clear in Fig. 6. The average and filter of multiple acquisitions can efficiently reduce the increased interferometric phase noise at large distances.

V. Experiment at the Grabengufer Rock Glacier

The GPRI was employed in August 2009 and March 2010 to measure the topographic change over the destabilized Grabengufer rock glacier in the Swiss southern Alps. Rock glaciers are large masses of perennially frozen ground supersaturated with ice affected by slow deformation and acting as sediment conveyors [18]. In the Alps, active rock glaciers above 2300 m above sea level are numerous. Their deformation rate lies typically on the order of 0.1 to 1.0 m/year. In response to the rapid increase in air temperature that occurred in the European Alps during the 1980s, permafrost has warmed by about 0.5 °C to 1 °C, and rock glaciers are moving significantly faster [19]. In the worst cases, the dramatic increase of the activity has initiated a landslide-like mass wasting phenomenon.

Measurements of the Grabengufer rock glacier were performed for about one day on each of the two observation periods from a distance of about 1 km. The time interval between subsequent acquisitions was on the order of 15 min. The array of antennas was rotated on the azimuthal axis by 40° in spacing of 0.1°. Single-pass interferograms were computed with one look in slant range and azimuth. Also in winter with the area covered by about 1 m of dry snow cover, we observe very well preserved fringes. Phase unwrapping was performed with a minimum-cost-flow algorithm after nonlinear phase filtering [15], [16]. Finally, the unwrapped phases were

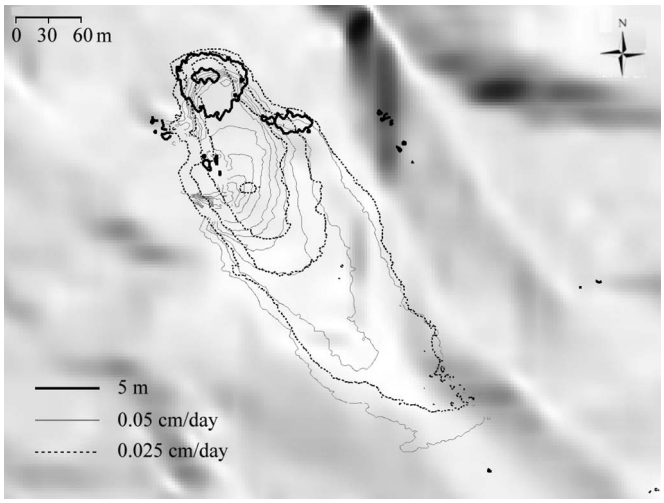

Fig. 7. Contour lines of the height difference measured with the terrestrial radar interferometer (bold black line) between August 2009 and March 2010 over the Grabengufer rock glacier overlaid onto the shaded relief of the external DEM. The contour lines of the displacement rates measured in (thin gray line) August 2009 and (dotted black line) March 2010 are also shown.

converted to surface topography with support of ground control points extracted from an external DEM. The contour lines of the height difference between the GPRI measurements of August 2009 and March 2010 are shown in Fig. 7. We can observe an increase of a maximum of 10 m of the surface topography from summer to winter at the front of the rock glacier. The contour lines of the displacement rates measured with the GPRI are also shown in Fig. 7. In summer, the highest displacement rate was larger than 40 cm/day. In winter, the rate of movement decreased to a maximum of 10 cm/day. Large quantities of loose material are accumulating at the snout of the rock glacier and will contribute during the melting season to the delivery of sediments in the underlying slope.

VI. Conclusion

We have presented an innovative concept of terrestrial radar interferometer for topographic reconstruction and its application to the measurement and interpretation of geophysical phenomena like glacier retreat and rock glacier destabilization. Broad interest of instrument, methods, and analysis presented in this letter is assured by the recent significant changes observed for most mountain regions around the world as a consequence of air temperature increase. In comparison to terrestrial laser scanners, the GPRI can be employed for a quick topographic reconstruction with reduced accuracy, along with the monitoring of surface displacement. The GPRI is illuminating the area of interest from a remote location, avoiding *in situ* installations required, for instance, for GPS measurements. Currently, we are advancing the GPRI prototype system into a new generation of instruments with a variety of improvements, making them robust and reliable for field surveys. Significant developments include greater weather resistance, greater stability in windy conditions, autonomous operation at temperatures between $-30\ ^{\circ}\mathrm{C}$ and $+45\ ^{\circ}\mathrm{C}$ over long periods, very fast image acquisition (a few seconds for a 180° scan), improved antenna design, and a built-in GPS-disciplined oscillator providing timing and frequency reference so that multiple radars can make simultaneous measurements.

Acknowledgment

DHM25 Rhonegletscher © 2007 swisstopo. DHM25 Grabengufer rock glacier © 2010 swisstopo. The authors would like to thank A. Bauder and M. Funk for the field support at Rhonegletscher and H. Raetzo and R. Delaloye for the field support at the Grabengufer rock glacier.

References

[1] C. Poidomani, D. Costantini, P. Pasquali, and P. Jaeger, "National-scale DEM generation using ERS Tandem data in alpine regions," in *Proc. ERS-ENVISAT Symp.*, Gothenburg, Sweden, Oct. 16–20, 2000.

[2] H. Pritchard, T. Murray, T. Strozzi, S. Barr, and A. Luckman, "Surge-related topographic change of the glacier Sortebræ, East Greenland, derived from synthetic aperture radar interferometry," *J. Glaciol.*, vol. 49, no. 166, pp. 381–390, Jan. 2003.

[3] H. Zebker, C. Werner, P. Rosen, and S. Hensley, "Accuracy of topographic maps derived from ERS-1 interferometric radar," *IEEE Trans. Geosci. Remote Sens.*, vol. 32, no. 4, pp. 823–836, Jul. 1994.

[4] I. Joughin, D. Winebrenner, M. Fahnestock, R. Kwok, and W. Krabill, "Measurement of ice-sheet topography using satellite radar interferometry," *J. Glaciol.*, vol. 42, no. 140, pp. 10–22, 1996.

[5] E. Rodriguez, C. Morris, J. Belz, E. Chapin, J. Martin, W. Daffer, and S. Hensley, "An assessment of the SRTM topographic products," Jet Propulsion Lab., Pasadena, California, Tech. Rep. JPL D-31639, 2005, 143 pp.

[6] B. Rabus, M. Eineder, A. Roth, and R. Bamler, "The Shuttle Radar Topography Mission—A new class of digital elevation models acquired by spaceborne radar," *ISPRS J. Photogramm. Remote Sens.*, vol. 57, no. 4, pp. 241–262, Feb. 2003.

[7] M. Pieraccini, G. Luzi, and C. Atzeni, "Terrain mapping by ground-based interferometric radar," *IEEE Trans. Geosci. Remote Sens.*, vol. 39, no. 10, pp. 2176–2181, Oct. 2001.

[8] G. Nico, D. Leva, G. Antonello, and D. Tarchi, "Ground-based SAR interferometry for terrain mapping: Theory and sensitivity analysis," *IEEE Trans. Geosci. Remote Sens.*, vol. 42, no. 6, pp. 1344–1350, Jun. 2004.

[9] G. Nico, D. Leva, J. Fortuny-Guasch, G. Antonello, and D. Tarchi, "Generation of digital terrain models with a ground-based SAR system," *IEEE Trans. Geosci. Remote Sens.*, vol. 43, no. 1, pp. 45–49, Jan. 2005.

[10] L. Noferini, M. Pieraccini, D. Mecatti, G. Macaluso, G. Luzi, and C. Atzeni, "DEM by ground based SAR interferometry," *IEEE Geosci. Remote Sens. Lett.* , vol. 4, no. 4, pp. 659–663, Oct. 2007.

[11] C. Werner, A. Wiesmann, T. Strozzi, and U. Wegmüller, "Gamma's portable radar interferometer," in *Proc. 13th FIG Int. Symp. Deformation Meas. Anal., 4th IAG Symp. Geodesy Geotech. Struct. Eng.*, Lisbon, Portugal, May 12–15, 2008, pp. 1–10.

[12] C. Werner, T. Strozzi, U. Wegmüller, and A. Wiesmann, "A real-aperture radar for ground-based differential interferometry," in *Proc. IGARSS*, Boston, MA, Jul. 6–11, 2008, pp. 1–2.

[13] R. Bamler and P. Hartl, "Synthetic aperture radar interferometry," *Inverse Probl.*, vol. 14, no. 4, pp. R1–R54, Aug. 1998.

[14] S. Sugiyama, A. Bauder, C. Zahno, and M. Funk, "Evolution of Rhonegletscher, Switzerland, over the past 125 years and in the future: Application of an improved flowline model," *Ann. Glaciol.*, vol. 46, no. 1, pp. 268–274, Oct. 2007.

[15] R. Goldstein and C. Werner, "Radar ice motion interferometry," in *Proc. 3rd ERS Symp.*, Florence, Italy, Mar. 18–21, 1997.

[16] C. Werner, U. Wegmüller, T. Strozzi, and A. Wiesmann, "Processing strategies for phase unwrapping for INSAR applications," in *Proc. EUSAR*, Cologne, Germany, Jun. 4–6, 2002.

[17] F. Paul and W. Haeberli, "Spatial variability of glacier elevation changes in the Swiss Alps obtained from two digital elevation models," *Geophys. Res. Lett.*, vol. 35, p. L21 502, 2008.

[18] W. Haeberli, B. Hallet, L. Arenson, R. Elconin, O. Humlum, A. Kääb, V. Kaufmann, B. Ladanyi, N. Matsuoka, S. Springman, and D. Vonder Mühll, "Permafrost creep and rock glacier dynamics," *Permafrost Periglacial Process.*, vol. 17, no. 3, pp. 189–214, Jul.–Sep. 2006.

[19] A. Kääb, R. Frauenfelder, and I. Roer, "On the response of rockglacier creep to surface temperature increase," *Global Planet. Change*, vol. 56, no. 1/2, pp. 172–187, 2007.